

Experimental and Numerical Analysis of the Tensile Test on the A633 HSLA Steel Plate Specimens with Edge Crack

Shahin Nayyeri Amiri¹, Caesar Abishdid², Asad Esmaeily³

¹Lecturer, Department of Civil Engineering, Kansas State University, Manhattan KS, USA,

²Associate Professor, Lebanese American University, Department of Civil Engineering, 211 E 46th St. New York, NY 10017, USA

³Professor, Department of Civil Engineering, Kansas State University, Manhattan KS, USA,

ABSTRACT: This paper presents an experimental and numerical study of the mechanical behavior of ASTM A633 high-strength low-alloy (HSLA) steel plate specimens with edge crack at the middle during the tensile test. Experimental analysis and numerical method are used to analyze the load-displacement curve for the steel specimens with various edge crack length. Four A633 HSLA steel plate specimens are tested in FIU's Material Laboratory using a high capacity universal testing machine, and results are compared with the mesh-free and finite element results. A mesh-free method called Reproducing Kernel Particle Method (RKPM) is used to calculate the J -integral and load-displacement. RKPM is a mesh-free technology which is used to analyze the domain of interest only with particles using Ramberg-Osgood stress-strain relationship. A numerical analysis was performed using the finite element program ANSYS to exhibit the efficacy of RKPM in analyzing crack problems. This paper studies the effect of crack length on the load-displacement curve and the J -integral of A633 HSLA specimens after tensile tests. Results of load-displacement curves and J -integral curves found using the experimental, finite element, and mesh-free methods were compared and validated against each other for samples with various crack lengths.

Keywords - Tensile Test, A633 HSLA, Steel Plate Specimens, Edge Crack, Reproducing Kernel Particle Method, Mesh-free Technology, Load-displacement Curve, J -integral, Finite Element Method.

I. INTRODUCTION

In recent years, mesh-free methods have been increasingly utilized in solving various types of boundary value problems. One of the oldest approaches used in mesh-free methods is the Smooth Particle Hydrodynamics (SPH), which was first introduced in 1977 by Lucy Gingold and Monaghan [3]. Recent advances in mesh-free methods are: element-free Galerkin method (EFGM) by Belytschko [4] et al at 1994,

reproducing kernel particle method (RKPM) by Liu, et al. [2] at 1996, and mesh-less local Petrov-Galerkin (MLPG) by Atluri, et al. [5] at 1999. Among these methods RKPM and EFG have been demonstrated as most suitable for studying crack problems in structural analysis.

In fracture mechanics problems, energy release rate is the energy dissipated during fracture. The concept of energy release rate was first introduced by Cherepanov (1967) and Eshelby (1970), but it was Rice [6] who first used this independent path integral in fracture mechanics problems. In 1968, Rice [6] presented the concept of energy release rate by means of J -integral. The J -integral represents a way to calculate the strain energy release rate, or work (energy) per unit fracture surface area, in a material. An important feature of the J -integral is that it is path independent and it helps to calculate the J -integral at a distance far from the crack tip. In linear-elastic fracture mechanics, the J -integral has a direct relationship with the stress intensity factors (SIFs). In this study the J -integral has been used to calculate the SIF at the crack tip.

Hugo Ernst [7] and et al. (1979) found the dimensional relationships between load, crack length, and plastic displacement in a cracked member or specimen. He also analyzed load-displacement relationships to determine J -R curve and material properties. David J. Macon [8] also found an expression for the J -integral of a nonlinear elastic material for an advancing crack in a tapered double cantilever beam fractured specimen and how these energies correlates to the crack position. That is why the J -integral and load-displacement curves are evaluated in this research at the same time using mesh-free and finite element methods.

To evaluate the load-displacement curve, a tensile test is needed to be carried out for the samples. The tensile test is an important and widely used test to

determine the mechanical properties of steel material. In a tensile test, a specimen is pulled and the specimen deformation and applied load are recorded until its fracture in order to draw the load-displacement and stress-strain curve. The stress-strain diagram indicates the yield strength, ultimate tensile strength, elastic modulus, and ductility of the material. Metals including carbon steel have a linear stress-strain relationship up to the yield point. In some steels the stress falls after the yield point. After the yield point, steel will undergo a period of strain hardening, in which the stress increases again with increasing strain up to the ultimate strength. If the material is unloaded at this point, the stress-strain curve will be parallel to that portion of the curve between the origin and the yield point [9, 10].

Celentano [11] presented a large strain thermo-viscoplastic formulation for the analysis of the solidification process of spheroidal graphite (S.G) cast iron in a green sand mold. This formulation includes two different non-associate constitutive models in order to describe the thermo mechanical behavior of each of such materials during the whole process. The performance of these models is evaluated in the analysis of a solidification test. Gozzi et. al [12] studied concerning the mechanical behavior of extra high strength steel. This is investigated by means of biaxial testing of flat cross-shaped specimens in the full σ_1 - σ_2 plane, a concept developed earlier at Steel Structures, Luleå University of Technology. Furthermore, new specimen designs had to be developed to enable testing of a material with high yield strength and low ultimate over yield strength ratio, such as the extra high strength steel Weldox 1100. The tests are performed in two steps: one initial loading followed by unloading and a subsequent loading in a new direction. The test results, containing data from 15 biaxial tests, are characterized by a slightly anisotropic initial yield criterion where the proof stress in compression is consequently somewhat higher compared to the results in tension.

The main objective of this work is to study the effect of crack length on the load-displacement curve of A633 HSLA specimens after tensile tests. This objective is evaluated using finite element method, meshless method and experimental work.

II. Reproducing Kernel Particle Method (RKPM)

SPH method first was introduced in 1977 by Lucy Gingold and Monaghan [3]. In the SPH method, system response is reproduced by invoking the notion of a kernel approximation for $f(x)$ on domain Ω by Equation (1):

$$u^R(\xi) = \int_{\Omega} \phi_a(\xi - x) u(x) d\Omega \quad (1)$$

where $u^R(\xi)$ is the approximation function, Ω is the domain of interest, $\phi_a(\xi-x)$ is a kernel function, and a is the dilation parameter. This method is not accurate on the boundary conditions, or when few particles are considered on the domain unless the lumped volume is carefully selected, which is very hard and time consuming. RKPM is an alternative method to formulate the discrete consistency that is lacking in the SPH method. The foundation of the RKPM was proposed by Liu et al. [2] in 1993 and applied to computational mechanics. RKPM modifies the kernel function by introducing a correction function $C(\xi; \xi-x)$. Adding the correction function in the kernel approximation significantly enhances the solution accuracy in comparison to the SPH method. The method of using corrected kernel approximation in reproducing a function is called Reproducing Kernel Particle Method. The reproduced kernel function of $u(x)$ can be written as Equation (2):

$$u^R(\xi) = \int_{\Omega} u(x) \bar{\phi}(\xi; \xi - x) dx \quad (2)$$

where $\bar{\phi}(\xi; \xi - x)$ is the modified kernel function on domain Ω that is expressed by Equation (3):

$$\bar{\phi}(\xi; \xi - x) = C(\xi; \xi - x) \phi(\xi - x) \quad (3)$$

$$\phi_a(\xi - x_i) = \frac{1}{a} \phi\left(\frac{\xi - x_i}{a}\right) \quad (4)$$

where $\phi_a(\xi - x)$ is window function, $C(\xi; \xi - x)$ is a correction function, and a is the dilation parameter of the kernel function. Dilation parameter is defined in order to give more flexibility for the window function, and it will also control the expansion of the window function on

the domain. The correction function $C(\xi; \xi - x)$ proposed by Liu et al. is shown by a linear combination of polynomial including some unknown coefficients. These unknown coefficients will be computed after imposing the boundary conditions. In order to get the equations for reproducing an arbitrary function, consider the following Taylor series expansion:

$$u(x) = \sum_{\alpha=0}^{\infty} \frac{(-1)^\alpha}{\alpha!} (\xi - x)^\alpha u^{(\alpha)}(\xi) \tag{5}$$

Substituting Equation (5) into Equation (2) leads to:

$$u^R(\xi) = \sum_{\alpha=0}^{\infty} \frac{(-1)^\alpha}{\alpha!} \left(\int_{\Omega} (\xi - x)^\alpha \bar{\phi}_a(\xi; \xi - x) dx \right) u^{(\alpha)}(\xi) \tag{6}$$

In order to simplify Equation (6), the α^{th} degree moment matrix of function $\bar{\phi}_a(\xi; \xi - x)$ is defined by:

$$\bar{m}_\alpha(\xi) = \int_{\Omega} (\xi - x)^\alpha \bar{\phi}_a(\xi; \xi - x) dx \tag{7}$$

Then Equation (6) will be rewritten in the form of Equation (8):

$$u^R(\xi) = \bar{m}_0(\xi)u(\xi) + \sum_{\alpha=1}^{\infty} \frac{(-1)^\alpha}{\alpha!} \bar{m}_\alpha(\xi)u^{(\alpha)}(\xi) \tag{8}$$

In order to exactly reproduce the n^{th} order polynomial function, the following conditions need to be satisfied;

$$\begin{cases} \bar{m}_0(\xi) = 1 \\ \bar{m}_\alpha(\xi) = 0 \quad \alpha = 1, 2, \dots, n \end{cases} \tag{9}$$

Or in summary:

$$\bar{m}_\alpha(\xi) = \delta_{\alpha 0} \quad ; \quad \alpha = 0, 1, 2, \dots, n \tag{10}$$

If a correction function including $n+1$ unknown coefficient is defined, $n+1$ Equations (10) can be satisfied simultaneously. The correction function is defined by Equation (11):

$$C(\xi, \xi - x) = \sum_{\alpha=0}^n \beta_\alpha(\xi) (\xi - x)^\alpha \tag{11}$$

It can be also expressed in matrix form:

$$C(\xi; \xi - x) = P^T(\xi - x)\beta(\xi) \tag{12}$$

where $P^T(\xi - x)$ is a set of basic functions and including $n+1$ components and $\beta(\xi)$ is a set of

unknown coefficient. Substituting Equation (12) into Equation (10) and considering definition of moment matrix in Equation (7) leads to Equation (13):

$$\int_{\Omega} \langle (\xi - x)^\alpha (\xi - x)^{\alpha+1} \dots (\xi - x)^{\alpha+n} \rangle \phi_n(\xi - x) dx \begin{Bmatrix} \beta_0(\xi) \\ \beta_1(\xi) \\ \vdots \\ \beta_n(\xi) \end{Bmatrix} = \delta_{\alpha 0} \quad \alpha = 1, 2, \dots, n \tag{13}$$

From Equation (13) the unknown coefficient sets of $\beta_i(\xi)$ are obtained. Equation (13) can also be rewritten as Equation (14).

$$\begin{Bmatrix} m_\alpha(\xi) & m_{\alpha+1}(\xi) & \dots & m_{\alpha+n}(\xi) \end{Bmatrix} \begin{Bmatrix} \beta_0(\xi) \\ \beta_1(\xi) \\ \vdots \\ \beta_n(\xi) \end{Bmatrix} = \delta_{\alpha 0} \tag{14}$$

Or it can be shown in matrix form as Equations (15) and (16):

$$\begin{bmatrix} m_0(\xi) & m_1(\xi) & \dots & m_n(\xi) \\ m_1(\xi) & m_2(\xi) & \dots & m_{n+1}(\xi) \\ \vdots & \vdots & \dots & \vdots \\ m_n(\xi) & m_{n+1}(\xi) & \dots & m_{2n}(\xi) \end{bmatrix} \begin{Bmatrix} \beta_0(\xi) \\ \beta_1(\xi) \\ \vdots \\ \beta_n(\xi) \end{Bmatrix} = \begin{Bmatrix} 1 \\ 0 \\ \vdots \\ 0 \end{Bmatrix} \tag{15}$$

$$M(\xi)\beta(\xi) = P(0) \tag{16}$$

Moment matrix M can be shown as Equation (17):

$$M(\xi) = \int_{\Omega} P(\xi - x)P^T(\xi - x)\phi_a(\xi - x)dx \tag{17}$$

Since the window function is always positive, all the components of moment matrix are linearly independent with respect to ϕ_a . Therefore, the moment matrix is nonsingular. Hence, simultaneously solving Equation (16), the unknown coefficient sets of $\beta_i(\xi)$ are obtained:

$$\beta(\xi) = M^{-1}(\xi)P(0) \tag{18}$$

After obtaining the unknown coefficient sets $\beta_i(\xi)$, the correction function can be easily calculated from Equation (11). After obtaining the unknown coefficient sets of $\beta_i(\xi)$, the correction function is determined and the function $u(x)$ or its derivatives can be obtained using the reproducing function. Equation (18) can be discretized in order to apply

to various problems. Equation (19) is the result of the discretization in the reproducing equation using the trapezoid integration method.

$$u^R(\xi) = \int_{\Omega} u(x)\bar{\phi}(\xi; \xi-x)dx = \sum_{i=1}^{NP} u(x_i)\bar{\phi}(\xi; \xi-x_i)\Delta x_i \quad (19)$$

where NP is the total number of particles distributed throughout the domain Ω . Equation (19) can be rewritten as Equation (20):

$$u^R(\xi) = \sum_{i=1}^{NP} \psi_i(\xi)u_i \quad (20)$$

and $\psi_i(\xi)$ is called shape function:

$$\psi_i(\xi) = P^T(\xi-x_i)\beta_i(\xi)\phi_a(\xi-x_i)\Delta x_i \quad (21)$$

where i is the particle number on the domain, x_i is the coordinate of that particle, $\phi_a(\xi-x)$ is the kernel function, and $\psi_i(\xi)$ is defined as the shape function of particle i with coordinate of ξ . Two most regular kernel functions which are used in mesh-free methods are the Gaussian and Spline functions. All the Spline functions are symmetric around $x=0$ axis. In this study, the cubic Spline function is employed as the kernel function, which is:

$$S^3(x) = \begin{cases} \frac{2}{3} - 4x^2 - 4x^3 & 0 \leq x < \frac{1}{2} \\ \frac{4}{3} - 4x + 4x^2 - \frac{4}{3}x^3 & \frac{1}{2} \leq x < 1 \\ 0 & x \geq 1 \end{cases} \quad (22)$$

By considering Equation (20) and deriving from the Equation (21) with respect to x_k , the definition

of the derivative of the i^{th} shape function becomes:

$$\psi_{i,xk}(\xi) = \{P_{,xk}^T(\xi-x_i)\beta_i(\xi)\phi_a(\xi-x_i) + P^T(\xi-x_i)\beta_{i,xk}(\xi)\phi_a(\xi-x_i) + P^T(\xi-x_i)\beta_i(\xi)\phi_{a,xk}(\xi-x_i)\}\Delta x_i \quad (23)$$

in two dimensional RKPM $\Delta x_i = \Delta S_i$, where ΔS_i is the area pertinent to the i^{th} particle. In a random distribution of particles, the computation of ΔS_i is problematic. Hence for simplicity $\Delta S_i = 1$ has been mainly incorporated in the literature [13].

III. Assessment of Plane-Strain Condition Using RKPM

The main purpose of fracture mechanics is to determine the status of cracks during different loading stages. Stress, strain, displacement, and energy fields are required to obtain a driving force for crack growth. SIF and J -integral are two important concepts of crack problems. SIF is used to quantify the stress field around the crack tip. Many methods have been developed to determine the stress intensity factor. One of these methods to calculate the stress intensity factor is the J -integral. If a node is considered with distance r and angle α with the x -axis in the vicinity of the crack edge, then the stress field in this node is calculated according to the Irwin method in different crack modes [14]. Therefore, stress field in the crack tip for linear elastic materials is calculated by Equation (24):

$$\sigma_{ij} = \frac{K}{\sqrt{2\pi r}} f_{ij}(\theta) \quad (24)$$

K parameter is the SIF for different modes in the crack tip, and shown K_I , K_{II} , and K_{III} are for the first, second and third mode. Values of these coefficients are determined according to the dimensions and loading condition of the problem. Therefore, the SIF relationship is calculated from the analysis of the geometrical and loading condition. K_I , K_{II} , and K_{III} are physically the intensity of force transfer at the crack tip due to creation of the crack in the material. SIF plays an important role as a failure parameter. Rice (1968) also showed that this integral has linear elastic attitude with the energy release rate and was independent of the path around a crack. The two-dimensional J -integral was defined as Equation (25):

$$J = \oint_{\Gamma} W dy - T_i \frac{\partial u_i}{\partial x} ds \quad (25)$$

where W is strain energy density, and u is the displacement vector. The strain energy density is given by:

$$W = \int_0^{\epsilon_{ij}} \sigma_{ij} d\epsilon_{ij} \quad (26)$$

And it can be represented equally by the alternate forms

$$J = \int_0^p \left(\frac{\partial \Delta}{\partial a} \right)_p dp = - \int_0^{\Delta} \left(\frac{\partial p}{\partial a} \right)_{\Delta} d\Delta \quad (27)$$

where Δ is the work producing of load point displacement for the load, P. In the analysis, it is convenient to divide J-integral into elastic and plastic parts, J_{el} and J_{pl} . then the J-integral form in Equation (27) may be written:

$$J = J_{el} + J_{pl}$$

$$J = \int_0^p \left(\frac{\partial \Delta_{el}}{\partial a} \right)_p dp + \int_0^p \left(\frac{\partial \Delta_{pl}}{\partial a} \right)_p dp \quad (28)$$

The first item in the Equation (28) is the linear-elastic component, and the second term is the nonlinear-plastic component. The second term in Equation (28) can be reinterpreted by referring to Figure 1. This Figure shows load-displacement curves for two different cracks sized a and $a+da$. The area between is noted to be $J_{pl}da$, which is integrated over elements of the area by [7]:

$$J_{pl} = \int_0^p \left(\frac{\partial \Delta_{pl}}{\partial a} \right)_p dp = - \int_0^{\Delta_{pl}} \left(\frac{\partial p}{\partial a} \right)_{\Delta_{pl}} d\Delta_{pl} \quad (29)$$

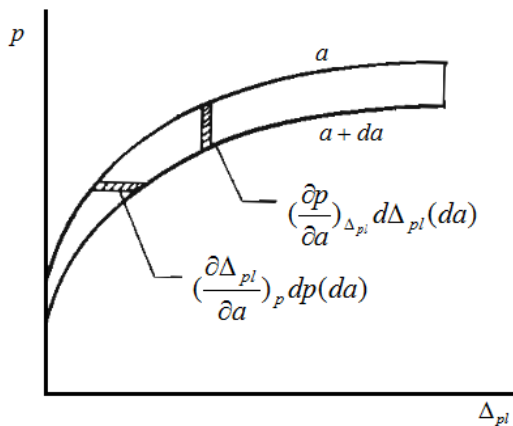


Figure 1: Load-displacement for two different crack lengths [7]

An important feature of the J-integral is that it is path-independent, and this helps to calculate the J-integral at a distance far from the crack tip. If Γ is considered as path-independent around an inclined

crack tip, which has angle of α with the x-axis, then the J-integral will be can be shown in matrix form as:

$$J = \int_{\Gamma} W d\eta - \int_{\Gamma} \left\{ \sigma_n \quad \tau_n \right\} \begin{bmatrix} \frac{\partial u_n}{\partial \xi} \\ \frac{\partial u_n}{\partial \eta} \\ \frac{\partial \xi}{\partial \xi} \end{bmatrix} ds \quad (30)$$

σ_n , and τ_n are the stresses in an arbitrary direction which has angle of α with x-axis.

$$\sigma_n = \sigma_{xx} \cos^2 \alpha + \sigma_{yy} \sin^2 \alpha + \tau_{xy} \sin \alpha \cos \alpha$$

$$\tau_n = (\sigma_{yy} - \sigma_{xx}) \sin \alpha \cos \alpha + \tau_{xy} (\cos^2 \alpha - \sin^2 \alpha) \quad (31)$$

u_n , and v_n are displacement in the same direction:

$$u_n = u \cos \alpha + v \sin \alpha$$

$$v_n = -u \sin \alpha + v \cos \alpha \quad (32)$$

Substituting Equations 31 and 32 in Equation 30 the J-integral will be easily calculated. Figure 2 shows that $Q_1Q_2Q_3Q_4$ is considered as a path for the J-integral in a fully elastic domain.

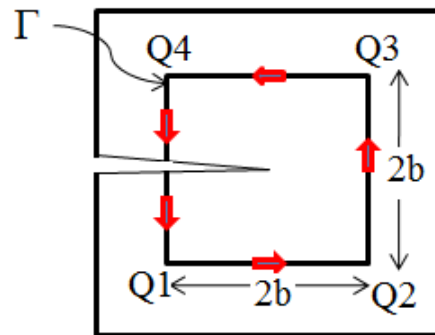


Figure 2: J-integral Path at the Crack Tip

First, the shape of the integral path is described, and then the value of integral is calculated on each separate path for two plane stress and plane strain condition. It is obvious that stress is $\sigma = D.\epsilon$ in elastic condition and it can be stated in matrix form:

$$\begin{Bmatrix} \sigma_{xx} \\ \sigma_{yy} \\ \sigma_{xy} \end{Bmatrix} = \begin{bmatrix} D_{11} & D_{12} & 0 \\ D_{12} & D_{22} & 0 \\ 0 & 0 & D_{11} \end{bmatrix} \begin{Bmatrix} \epsilon_{xx} \\ \epsilon_{yy} \\ \epsilon_{xy} \end{Bmatrix} = \begin{bmatrix} D_{11}\epsilon_{xx} + D_{12}\epsilon_{yy} \\ D_{12}\epsilon_{xx} + D_{22}\epsilon_{yy} \\ D_{33}\epsilon_{xy} \end{bmatrix} \quad (33)$$

Then strain energy density is calculated from:

$$W = \frac{1}{2} \sigma^T \varepsilon \quad (34)$$

Substituting Equation (33) in Equation (34), strain energy density will be:

$$W = \frac{1}{2} \varepsilon_{xx} (D_{11} \varepsilon_{xx} + D_{12} \varepsilon_{yy}) + \frac{1}{3} \varepsilon_{yy} (D_{12} \varepsilon_{xx} + D_{22} \varepsilon_{yy}) + \frac{1}{2} D_{33} \varepsilon_{xy}^2$$

$$W = \frac{1}{2} D_{11} \varepsilon_{xx}^2 + \frac{1}{2} D_{22} \varepsilon_{yy}^2 + D_{12} \varepsilon_{xx} \varepsilon_{yy} + \frac{1}{2} D_{33} \varepsilon_{xy}^2 \quad (34)$$

And the J -integral on the closed path is:

$$J = \int Q_1 Q_2 + \int Q_2 Q_3 + \int Q_3 Q_4 + \int Q_4 Q_1 \quad (35)$$

With what was stated previously, and using a FORTRAN program that was written for solving the liner-elastic on a steel plate with specified dimension using RKPM, the stress, strain, and displacement fields in x and y directions in all computational particles and the J -integral under plane-strain conditions are obtained. Penalty method is used to apply the boundary conditions. Penalty coefficient, β , is adopted as $10^6 E$, in which E is Young's modulus. To construct the shape functions in the vicinity of the crack and crack-tip, the diffraction criterion is employed and the crack tip region is also refined using more particles arrangements. A rectangular steel plate is selected with dimensions of $0.5 \times 1.5 \text{ in}^2$. An edge crack is considered with various crack length in the middle of the plate. A tensile stress of 60 ksi is applied at the bottom and the top of the plate. The loading increment is set to 5 ksi. Roller constraint is used for the plane in front of the crack, and pin constraint is used for the front face of the plate (Figure 3a). Spline 3rd degree is used as a window function. The modulus of elasticity of the plate is 30,000 ksi, Poisson ratio of 0.3 and hardening parameter $n=10$. The problem is investigated with 800 particles uniformly scattered on the surface of the plate, and 72 particles positioned on the circles with angles of 30 degree around the crack tip as shown in Figure 3b. Figure 4 shows the load-displacement curve for various crack length using RKPM.

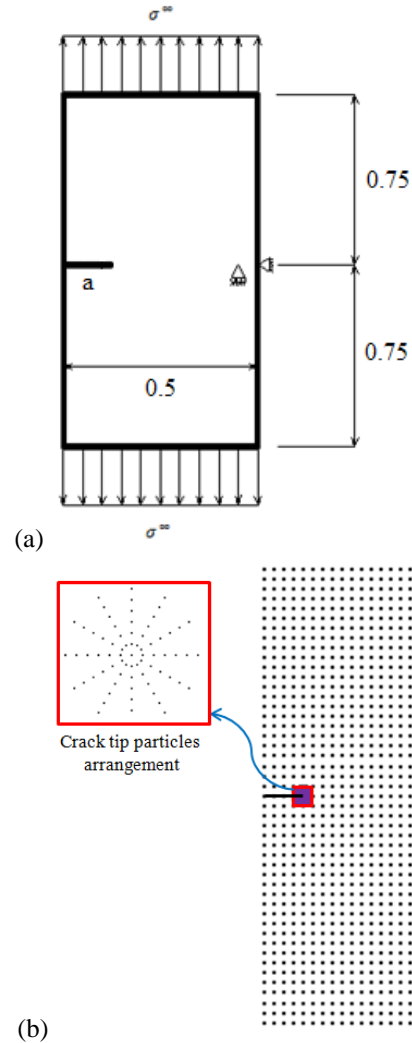


Figure 3: (a) Domain and Boundary Conditions, (b) Particle Arrangement

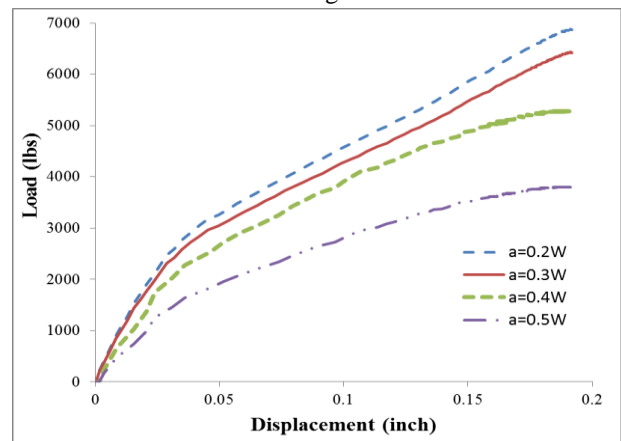


Figure 4: Load-displacement Curve, RKPM Results

IV. Finite Element Model

A numerical analysis was performed using the finite element program ANSYS12 to exhibit the efficacy of RKPM in analyzing crack problems. The model considered the measured geometry,

material properties and initial edge crack at the middle of the plate. Quadratic plane strain elements were used throughout the entire domain with a mesh size of 0.01×0.01 . Ideal boundary conditions were chosen as shown in Figure 3. A cubic steel plate is selected with dimensions of $1.27 \times 3.81 \text{ cm}^2$ ($1.5 \times 0.5 \text{ in}^2$) and thickness of 0.64 cm (0.25 inch) as shown in Figure 5. An edge crack is considered with various lengths of 0.254 , 0.381 , 0.508 , and 0.635 cm (0.1 , 0.15 , 0.2 and 0.25 inch) in the middle of the plate. A tensile force of 35.6 KN (8000 lbs) is applied at the bottom and the top of the plate. Thirteen thousand and forty five (13045) elements are used for the sample with $0.2W$ crack length. One quarter ($1/4$) of the sample is modeled in ANSYS and finer mesh is used in the crack tip (Figure 6). Figures 7 and 8 show the stress and displacement contour in Y-direction throughout the plate for samples with $0.2W$ and $0.4W$ crack lengths using ANSYS. Figure 9 shows the load-displacement curve for various crack length using FEM.

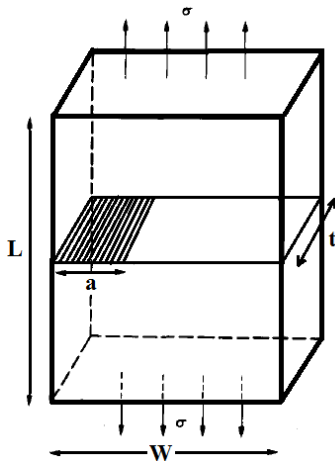


Figure 5: 3-dimensional Crack Modeling in ANSYS

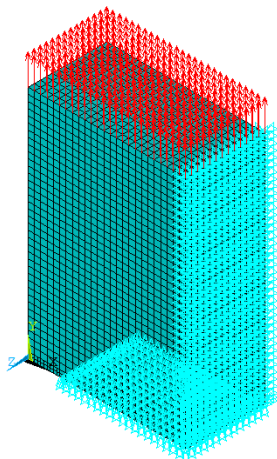
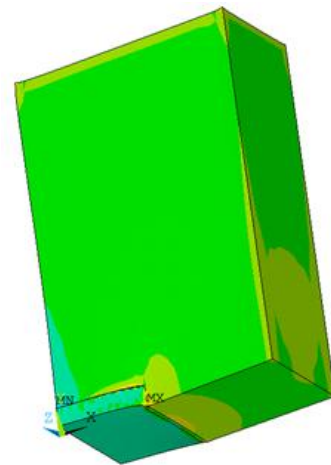


Figure 6: Meshing and Boundary Condition

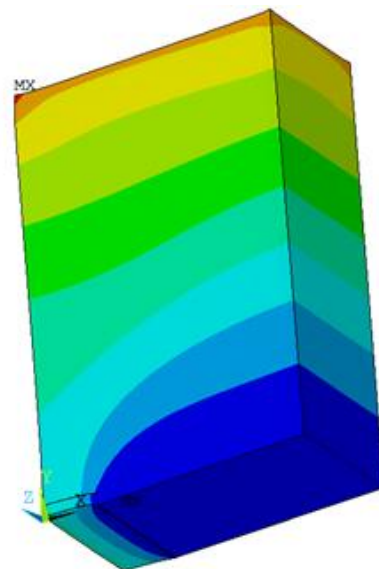


(a) $a=0.2W$

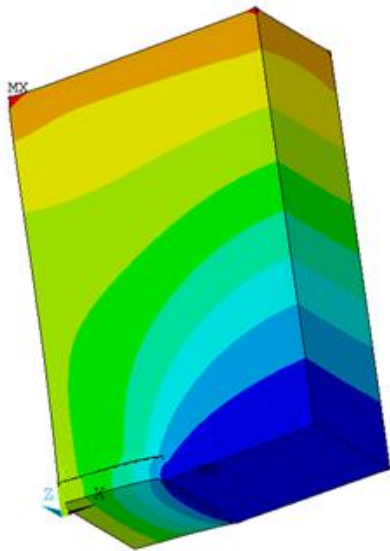


(b) $a=0.4W$

Figure 7: Stress Contours in Y-direction



(c) $a=0.2W$



(d) $a=0.4W$

Figure 8: Displacement Contours in Y-direction

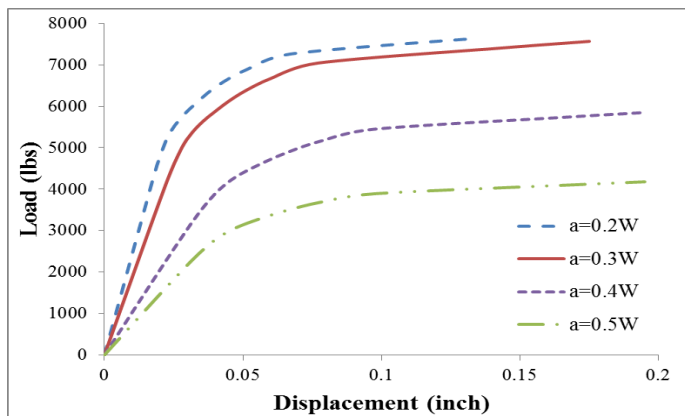


Figure 9: Load-displacement Curve, Finite Element Results

Figure 10 shows the J-integral value for various crack length using FEM and RKPM. It can be seen that the FEM results are higher than RKPM for J-integral values.

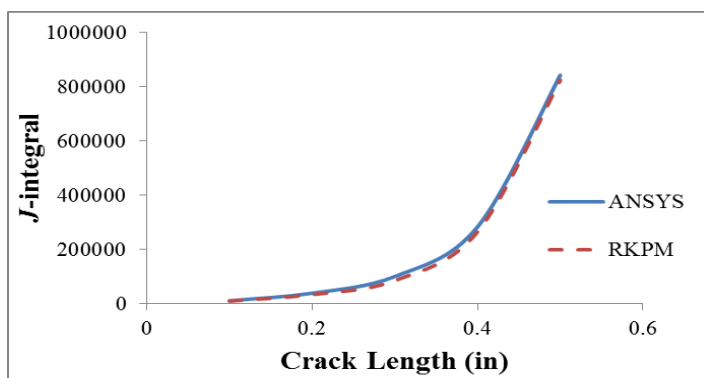


Figure 10: J-integral versus Crack Length using FEM and RKPM

Experimental Work

In the laboratory, four steel samples are tested using a high capacity universal testing machine shown in Figure 12. The tests were run at a constant displacement rate of 0.8 mm/sec. The width of the plates is 0.5 in and their length is 1.5 in with 0.25 inch thicknesses. Tests were carried out on four samples with various crack lengths: (a is the crack length and W is the width of the plate)

Sample A1: $a=0.2W$, Sample A2: $a=0.3W$, Sample A3: $a=0.4W$, Sample A4: $a=0.5W$



Figure 11: Samples A1 ($a=0.2W$), A3 ($a=0.4W$)

The steel specimens with the edge crack were tested using a universal testing machine at FIU's Material Laboratory. This machine is designed for accurate testing under axial loads (tensile and compression testing) up to 31 kN (7000 lbs) with standard displacements of 100 mm (3.94 in) as shown in Figure 9. The plate dimensions were 2 cm in length, 1 cm in width, 0.5 cm in thickness with an edge crack length of 0.2 cm. The steel material is ASTM A36 with yield strength of 250 MPa (36 ksi), and ultimate strength of 400 MPa (58 ksi) [1]. The plate was tested with a rate of 0.8 mm/sec, and a maximum force of 30 kN. Figures 13 through 17 shows the force versus displacement plots for this plate.



Figure 12: Universal Tensile Testing Machine

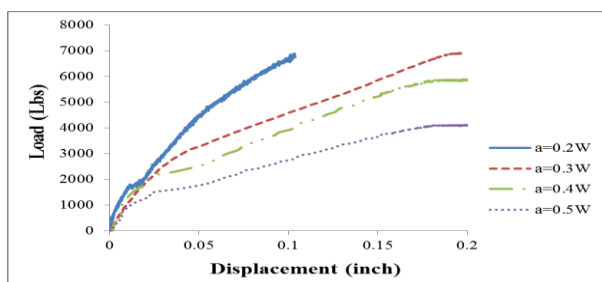


Figure 13: Load-displacement Curve, Experimental Results

Figure 14 shows the ultimate load of the A633 HSLA samples with various crack lengths. The experimental results show that the ultimate strengths of samples A1 and A2 is 12.5 percent, of sample A3 is 25 percent, and of sample A4 is 50 percent less than that of the sample without any cracks.

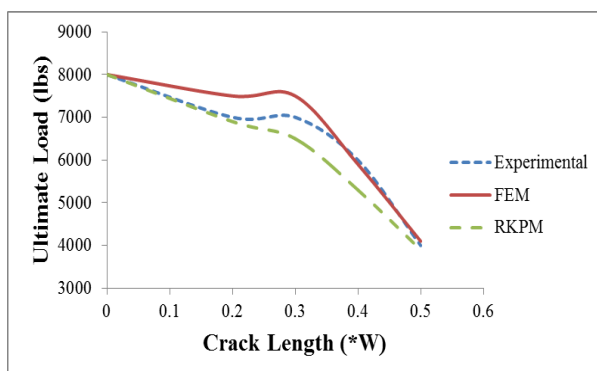


Figure 14: Ultimate Load versus Crack Length

V. CONCLUSION

The results of load displacement curves found using the experimental, finite element and mesh-free methods for samples with various crack lengths were found to be consistent. The yield strength, ultimate tensile strength, and fracture

stress showed to decrease with the increase in the crack length.

The ultimate load of A633 HSLA samples with various crack lengths was shown. The experimental results show that the ultimate tensile strengths of samples A1 and A2 is 12.5 percent, A3 is 25 percent, and A4 is 50 percent less than the ultimate tensile strength of sample without crack.

The *J*-integral, which is the energy discharge rate for a fully elastic analysis is less than the elastic-plastic analysis using the Ramberg-Osgood model. The reason is that in the elastic-plastic condition, the material at the crack tip experiences more strain than in the fully elastic condition, and more energy discharge for very small crack growth.

VI. Acknowledgements

The experiments were carried out at the Mechanical Engineering Department laboratory of the Florida International University. The writers thank Dr. Kuang-His Wu, professor in mechanical engineering department at FIU, for his assistance during the experimental testing in his laboratory. The first writer is also thankful to the University Graduate School for providing him with a *Doctoral Evidence Acquisition* fellowship in spring 2011 semester to complete his doctoral work.

REFERENCES

1. ASTM, ASTM E1820-09. Standard Test Method for Measurement of Fracture Toughness. American Society for Testing and Materials, Philadelphia, 2009.
2. Liu W K, Jun S, Zhang YF (1995). Reproducing Kernel Particles Methods. International Journal for Numerical Methods in Fluids, vol. 20, pp. 1081-1106.
3. Gingold RA and Monaghan JJ (1977). Smoothed particle hydrodynamics: theory and application to non-spherical stars." Monthly Notices Royal Astronomical Society, Vol. 181, pp. 375-389.
4. Belytschko T, Y Krongauz, D Organ, M Fleming, P Krysl, (1996). Meshless Methods: An overview and recent developments Computer methods in applied mechanics and engineering, Vol 139, pp3-47.
5. Zhu T, Atluri S N (1998). A modified collocation method and a penalty formulation for enforcing the essential boundary conditions in the element free Galerkin method. Computational Mechanics, vol. 21, pp. 211-222.
6. Rice J R (1968). A path independent integral and the approximate analysis of strain concentration by notches and cracks. Journal of Applied Mech., vol. 35, pp. 379-386.
7. Ernst H A, Paris P C, Rossow M, Hutchinson J W, (1979). Analysis of load displacement relationship to determine J-R curve and tearing instability material properties. Fracture Mechanics. ASTM STP 677, C. W. Smith, Ed.,

- American Society for Testing and Materials, Philadelphia, pp. 581-599.
8. Macon D J (2006). Nonlinear Elastic J-Integral Measurements in Mode I Using a Tapered Double Cantilever Beam Geometry. *Mathematical and Computer Science*, pp 33.
 9. Vinnakota S (2006). *Steel Structures: Behavior and LRFD*. McGraw-Hill, 1 st Edition, pp. 29-46.
 10. Ashby M (2006). *Engineering Materials 1: An Introduction to Properties, Applications and Design*. 3rd ed. Butterworth-Heinemann.
 11. Celentano DJ, (2001). A Large Strain Thermoviscoplastic Formulation for the Solidification of S.G.Cast iron in a green sand mould, *International journal of Plasticity*, Vol.17, pp.1623-1658.
 12. Gozzi J, Olsson A, and Lagerqvist O (2005). Experimental investigation of the behavior of extra high strength steel. *Experimental Mechanics*. Volume 45, Number 6, p. 533-540.
 13. Jin X, Li G, Aluru, N R (2001). On the equivalence between leastsquares and kernel approximations in meshless methods. *CMES: Computer Modeling in Engineering & Sciences*, vol. 2, pp. 447-462.
 14. Jacobsen TK, Sorensen BF (2001). Mode I intra-laminar crack growth in composites modeling of R-curves from measured bridging laws. *Composites Part A.*, 32: 1-11.
 15. Cao R, Li L, Chen JH, Zhang J, (2010). Study on compression deformation, damage and fracture behavior of TiAl alloys Part II. Fracture behavior, *Materials Science and Engineering A* 527 2468–2477.
 16. Xia L, Shih F, Hutchinson JW, (1995). A computational approach to ductile crack growth under large-scale yielding conditions. *Journal of Mech Phys Solids*, 43:389–413.
 17. Simonsen BC, Lauridsen LP, (2000). Energy absorption and ductile failure in metal sheets under lateral indentation by a sphere. *Int J Impact Eng*, 24:1017–39.
 18. Panda S K, Kumar, D R, Kumar, H, Nath, AK (2007). Characterization of tensile properties of tailor welded IF steel sheets and their formability in stretch forming, *Journal of Materials Processing Technology* 183, 321–332.
 19. Grønwoold E (2003). Experimental set-up for large-scale fracture mechanics testing. Master thesis, Department of Mechanical Engineering, Maritime Engineering, and Technical University of Denmark.
 20. Hajali, M., & Abishdid, C. (2013). Determination of Two-Dimensional Plastic Zone Shape and SIF at Crack-Tip Using RKPM. *Journal of Iron and Steel Research, International*, 20(12), 103-114.
 21. Hajali, M., Abishdid, C., Johansson, S., & Moverare, J. (2013, March). 126 Evaluation of the Mode I Plastic Zone Size at the Crack Tip Using RKPM and FEM. In *CP2012*.
 22. Hajali, M., & Abishdid, C. (2012, January). Effect of Dilation Parameter On the Stress Intensity Factor At the Crack Tip Using RKPM. In *46th US Rock Mechanics/Geomechanics Symposium*. American Rock Mechanics Association.